ARTICLE

MOF-derived Co₃O₄/Nitrogen-doped Carbon Composite for Chlorine-assisted Production of Ethylene Oxide

Received 00th January 20xx, Accepted 00th January 20xx

DOI: 10.1039/x0xx00000x

Tianlei Li^a, Hengzhou Liu^a, Jiaqi Yu^b, Yifu Chen^a, Wenyu Huang^b, Wenzhen Li^a*

Ethylene oxide (EO) is one of the most crucial materials in plastic industries. The traditional catalytic process requires high temperature and pressure to produce EO. A chlorine-assisted system has been reported to produce EO, but it required noble metal catalysts, which significantly increased the cost. In this work, a MOF-derived Co_3O_4 /nitrogen-doped carbon composite (Co_3O_4 /NC) prepared through a two-step calcination method has demonstrated remarkable chlorine evolution reaction (CIER) activity as compared with a commercial RuO_2 catalyst, which can be attributed to higher specific surface area and lower resistance of its porous structure and nitrogen-doped carbon. Further, the Co_3O_4 /NC maintained a stable potential and a high faradaic efficiency throughout the 10-hour electrolysis test.

Introduction

Ethylene oxide (EO), one of the most crucial chemicals for manufacturing consumer products and intermediates, was mass-produced with an annual production of over 34.5 Mt (2021) 1 . Taking great advantage of its strained ring structure, EO can participate in various addition reactions to open the ring. One major use of EO is its conversion to ethylene glycol 2 , which is one of the most important precursors in the plastic industry. In addition, EO can be used to produce ethanol amines 3 and various polymers with novel architectures 4 . Patented by Lefort in 1935 5 and numerous follow-up studies 6 - 9 , ethylene can be directly oxidized to EO on silver-based catalysts through thermal catalytic processes. However, relatively high temperature (220 $^\sim$ 280 $^\circ$ C) and high pressure (1 $^\sim$ 3 MPa) are required for this chemical transformation 10 .

Alternatively, EO can be produced by a chlorohydrin process (RXN 2,3,5)2. Powered by renewable electricity generated from solar and wind sources, chlorine (Cl₂) can be in-situ generated through the electrochemical process under ambient conditions (RXN 1). Then, EO can be produced from a chlorine-assisted process in the formation of ethylene chlorohydrin (RXN 2-3), followed by its chemical reaction with OH⁻ that was accumulated at the cathode (RXN 4) to produce ethylene oxide via a dehydrochlorination process (RXN 5) (Fig. 1a). At the meantime, hydrogen is generated on the cathode. 11 Iridium oxide (IrO₂) ¹² and barium oxide-loaded IrO₂ ¹³ were reported to achieve EO production with high faradaic efficiency (FE) of >70%. Besides, the dimensional stable anode (DSA), made of ruthenium oxide and titanium oxide, has been proven as an active and durable catalyst for Cl₂ evolution reaction (CIER) and is expected to be active for the chlorine-assisted EO generation process¹⁴. However, all those catalysts are based on noble metals, which significantly increases the overall process costs. Exploration of low-cost, robust, non-noble metal catalysts is highly desirable. Although several works showed that non-noble cobalt oxide (Co_3O_4) was an active and durable catalyst in the CIER process¹⁵⁻¹⁷, their performances are generally inferior to noble metal-based catalysts.

$$2Cl^{-} + 2e^{-} \rightarrow Cl_{2} \tag{1}$$

$$Cl_2 + H_2O \rightarrow HCI + HCIO$$
 (2)

$$HCIO + C_2H_4 \rightarrow CI-C_2H_4-OH$$
 (3)

$$2H_2O - 2e^- \rightarrow H_2 + 2OH^-$$
 (4)

$$CI-C_2H_4-OH + OH^- \rightarrow C_2H_4O + CI^- + H_2O$$
 (5)

In this work, a metal-organic framework (MOF)-derived porous cobalt oxide/nitrogen-doped carbon composite (Co₃O₄/NC) was studied for chlorine-assisted EO production. MOF-derived materials are well known for their unique porous structure that can offer high specific area that is desirable for various applications, such as sensing, energy storage and catalysis¹⁸⁻²⁰. However, they have been rarely studied for chlorine evolution reaction (CIER). Benefiting from the highly porous structure and carbonized organic linker of MOF as sacrificing template, Co₃O₄ catalysts with high specific surface area and low charge transfer resistance were prepared. Compared to the generally used direct calcination in the air to turn MOF into metal oxides, we investigated a two-step calcination method and observed that the calcination method and temperature significantly influenced the structure and CIER activity. The optimized catalyst has exhibited comparable CIER catalytic activities to commercial ruthenium oxide (RuO₂) catalyst, while the Co₃O₄ costs two orders of magnitude lower than RuO₂. Finally, the Co₃O₄/NC exhibited long-term durability for chlorine-assisted EO production.

Results and Discussion

Characterization of MOF-derived Co₃O₄

a. Department of Chemical and Biological Engineering, Iowa State University, 618 Bissell Road, Ames, IA 50011, USA. b. Chemistry Department, Iowa State University, 1605 Gilman Hall, Ames, IA 50011, USA. E-mail: wzli@iastate.edu

† Footnotes relating to the title and/or authors should appear here. Electronic Supplementary Information (ESI) available: [details of any supplementary information available should be included here]. See DOI: 10.1039/x0xx00000x

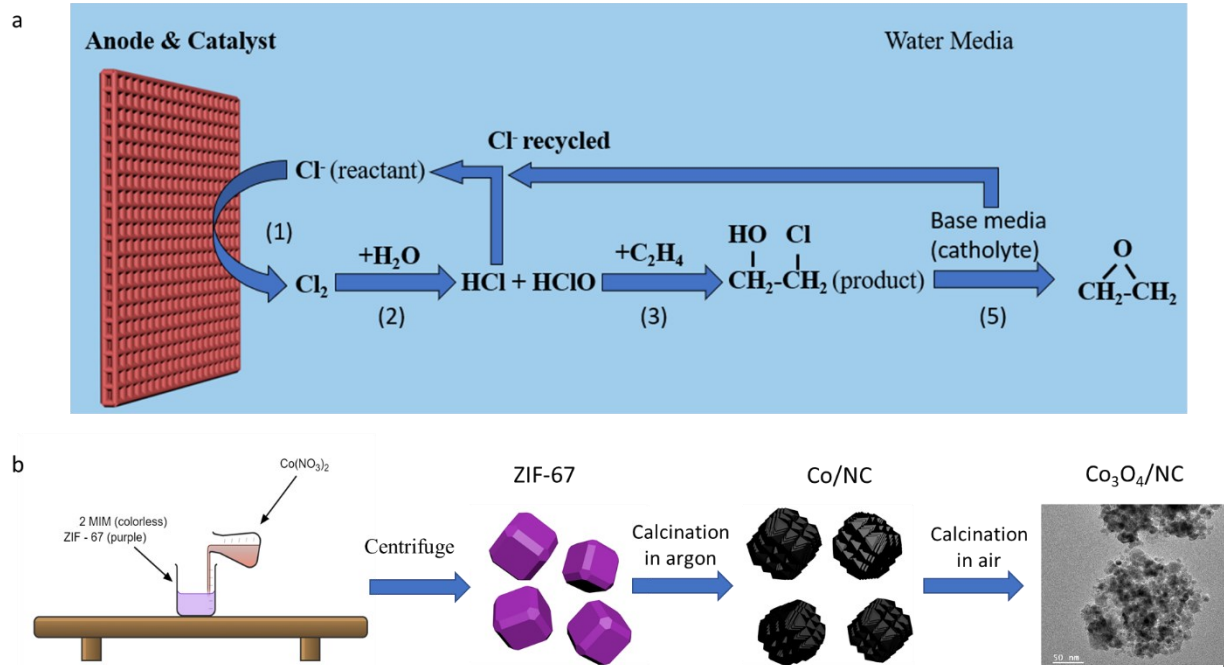


Figure 1. a) Scheme of the chlorine-assisted EO generation process, b) Synthesis process

Cobalt containing zeolite imidazole framework (ZIF-67) was chosen as the sacrificing template due to its facile hydrothermal synthesis process and nitrogen containing organic linker. MOF-derived Co₃O₄/NC samples were prepared from a two-step calcination treatment of ZIF-67. (Fig. 1b). Samples are named after thermal treatment temperatures. For example, ZCO-700-300 (ZCO is short for ZIF-derived cobalt oxide) was obtained by calcinating ZIF-67 at 700 °C under argon for 1 hour, followed by calcination at 300 °C in the air for 1 hour. The morphology and crystal structure of the pristine ZIF-67 after the hydrothermal synthesis were characterized by SEM (Fig. 2a) and XRD (Fig. 2d), showing a typical polyhedral morphology with the particle size of 150-200 nm²¹. After the first calcination step at 700 °C in argon atmosphere, SEM (Fig. 2b) showed a slight decrease in the particle size (~100 nm). XRD (Fig. 2e) indicated the transformation of ZIF-67 into metallic Co, and the organic linker was converted to nitrogen-doped carbon (Fig. S1a). The pore size distribution was well maintained after the first step calcination at 700 °C (Fig. S2a). Therefore, the first step temperature was not further optimized. The metallic Co/NC can be further converted into desirable Co₃O₄/NC through the second calcination step in the air, which shows a similar size to the sample after first step calcination as evidenced by SEM (Fig. 2c). The successful conversion of metallic Co into Co₃O₄ was also supported by XRD patterns (Fig. 2f), and XPS fitting spectra further suggested the existence of C-N bond (Fig. S3).

As the temperature of second thermal treatment largely affects the content species and porous structure **(Fig. S1, S2)**, it is critical to optimize its operating temperature. An extremely high temperature could collapse the small pores of MOF and remove nitrogen-doped carbon, but a relatively low temperature would not fully oxidize Co to Co_3O_4 . We kept the first step calcination temperature at 700 °C in argon and optimized the second step calcination temperature in air. As suggested by the TGA and TPO curves **(Fig. S4)**, ZCO-700-NA (NA indicates the second step has not been done yet) starts to decompose at 250 °C while ZIF-67 starts to decompose at 350 °C. As such, the second step of calcination was designed to perform at 250,

300 and 350 °C. To compare our developed two-step method with the generally used one-step method, samples were prepared via one-step calcination at 350 and 400 °C in the air. If the second step temperature is lower than 300 °C, Co can only be partially oxidized into Co₃O₄. For instance, as shown in the XRD patterns (Fig. S5), ZCO-700-250 possesses both Co and Co₃O₄ phases, as compared to ZCO-700-300 with a solely Co₃O₄ phase (Fig. 2f). Further increasing the second step temperature to 350 °C would decompose all the nitrogen-doped carbon, as shown in TGA and TPO curves (Fig. S4), which could undesirably increase the internal resistance of metal oxide catalysts. Energy dispersive spectroscopy (EDS) (Fig. S1) and TGA (Table S1) were performed to further confirm the species composition after the calcination at different temperatures. EDS and TGA showed a similar trend: with the second step calcination temperature increasing, a reduction in the amount of carbon and nitrogen was observed, along with an increase in the active content of Co₃O₄. With the second step calcination temperature over 300 °C (i.e., ZCO-700-300 and ZCO-700-350), the samples showed similar oxygen to Co ratio, indicating that Co was fully oxidized to Co₃O₄, and 300 °C was the ideal temperature for the second step calcination.

To further understand how temperature affects the pore size distribution and surface area of ZCO samples, nitrogen physisorption was performed. BET curves and pore size distributions were shown in **Fig. S2**. All samples showed a type IV hysteresis loops **(Fig. S2a)**, which indicates their mesoporous structures. As the second step calcination temperature increasing, large-size pores appeared with an increase in their portion **(Fig. S2b)**. BET surface area measured by nitrogen physisorption showed that the original pore structure in the ZIF-67 precursor collapsed during the calcination treatment, leading to a decrease in surface area **(Table S1)**. Therefore, the optimized second step calcination temperature is 300 °C, consistent with the EDS and TGA suggestions. TEM image of the ZCO-700-300 showed a d-spacing of 0.243 nm **(Fig. 2i)**, which can be assigned to the Co₃O₄ **(311)** plane, in line with the XRD results. The above synthesis and

Journal Name ARTICLE

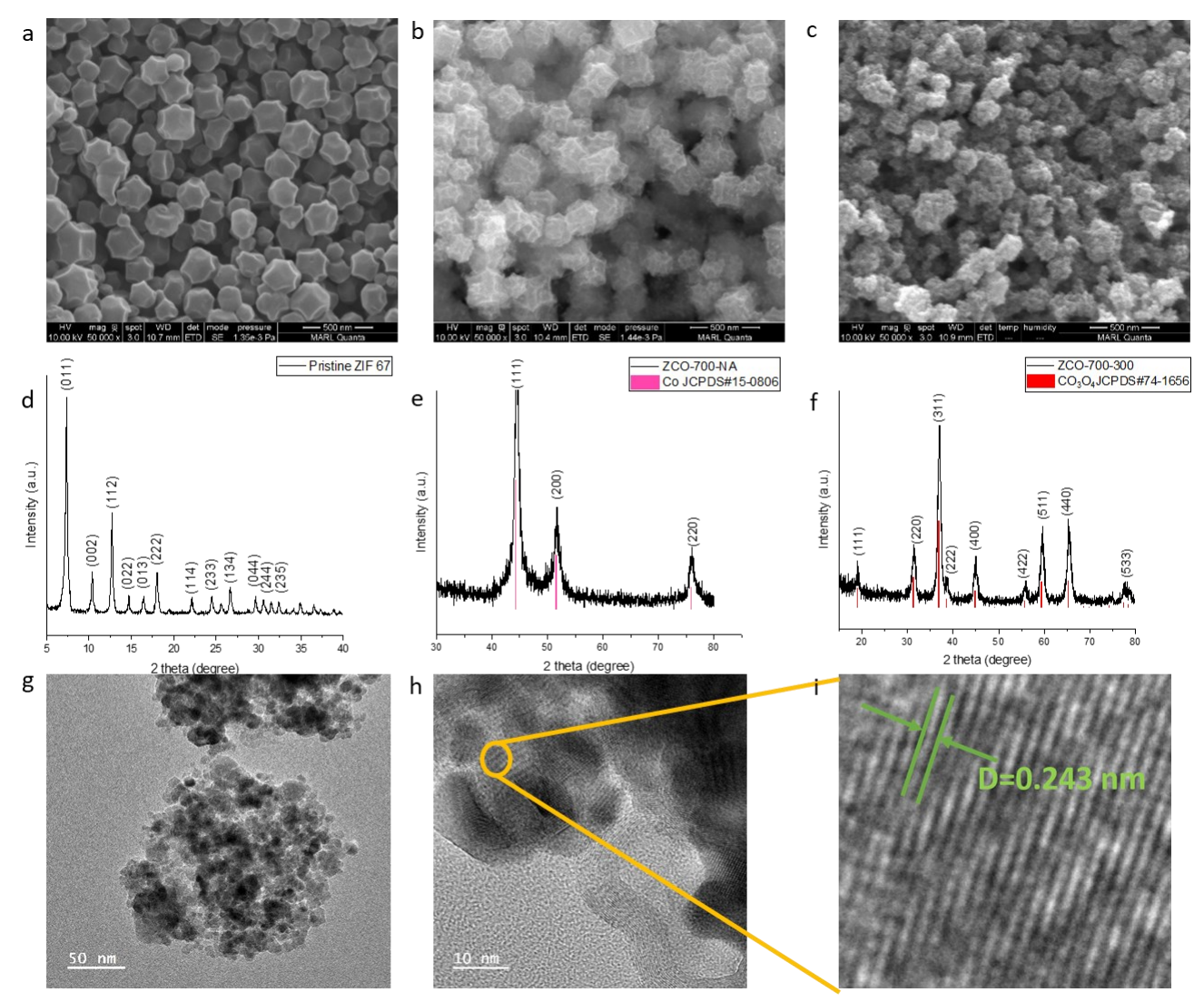


Figure 2. Characterization of catalysts. SEM images and XRD patterns of a,d) as-synthesized ZIF-67, b,e) ZCO-700-NA, and c,f) ZCO-700-300. g,h) TEM images of ZCO-700-300 at different magnifications. i) A zoom-in image of Figure 2h.

characterization results showed the successful preparation of MOF-derived $\text{Co}_3\text{O}_4.$

Electrochemical measurements on MOF-derived Co₃O₄

Performance comparisons are evaluated by linear scan voltammetry (LSV), as shown in Fig. 3a, S6. ZCO-700-300 exhibited comparable performance to RuO₂, and superior to commercial Co₃O₄ (C-Co₃O₄). At 100 mA/cm², only 0.04 V difference in CIER was observed between RuO_2 and ZCO-700-300. Similar kinetics between ZCO-700-300 and RuO₂ was also supported by examining their Tafel slopes (Fig. 3b). The potential dependence of the CIER on ZCO-700-300 was also investigated. The FE of EO (FEEO) and current density increased by positively shifting the anodic potential, and the FE_{EO} maintained >70% at the potential of >1.22 V vs. Ag/AgCl (Fig. S7). No active chlorine was detected in the absorbing vessel, and the ethylene chlorohydrin amount in the absorbing vessel was <1% in the anolyte. We reasoned that this was due to the facile reaction between ethylene and hypochlorous acid (HClO). Since HClO was consumed, the reversible reaction between chlorine gas and water will always favour production of HCl and HClO, with negligible chlorine escaped from the anolyte. Furthermore, by comparing the samples prepared

by different calcination temperatures, the sample with the second step calcination temperature of 300 °C showed a superior performance to other samples (Fig. 3c), consistent with our characterizations that Co was not only fully oxidized to Co₃O₄, but also maintained a better porous structure with optimal nitrogen doped carbon content. EIS tests were further carried out on these samples to compare the charge transfer resistance (Fig. 3d). ZCO-700-300 showed the lowest charge transfer resistance, contributing to its good CIER activity. Although ZCO-700-250 possessed both high surface area and low charge transfer resistance, Co was not fully oxidized to Co₃O₄ and the remaining Co could transform to Co(OH)₂ in the aqueous electrolyte under an anodic potential. XPS confirmed the presence of $Co(OH)_2$ species in the ZCO-700-250 sample (Fig. S8). It has been known that Co(OH)₂ is an active oxygen evolution reaction (OER) catalyst²², which is the main side reaction competing for CIER. This can be the reason to the decreased activity and selectivity of CIER on ZCO-700-250. At the second step calcination temperature of > 300 °C, a lower CIER performance could be due to the decrease in surface area (Table S1) and increase in internal resistance. Taken all together, the optimized MOF-derived Co₃O₄/NC

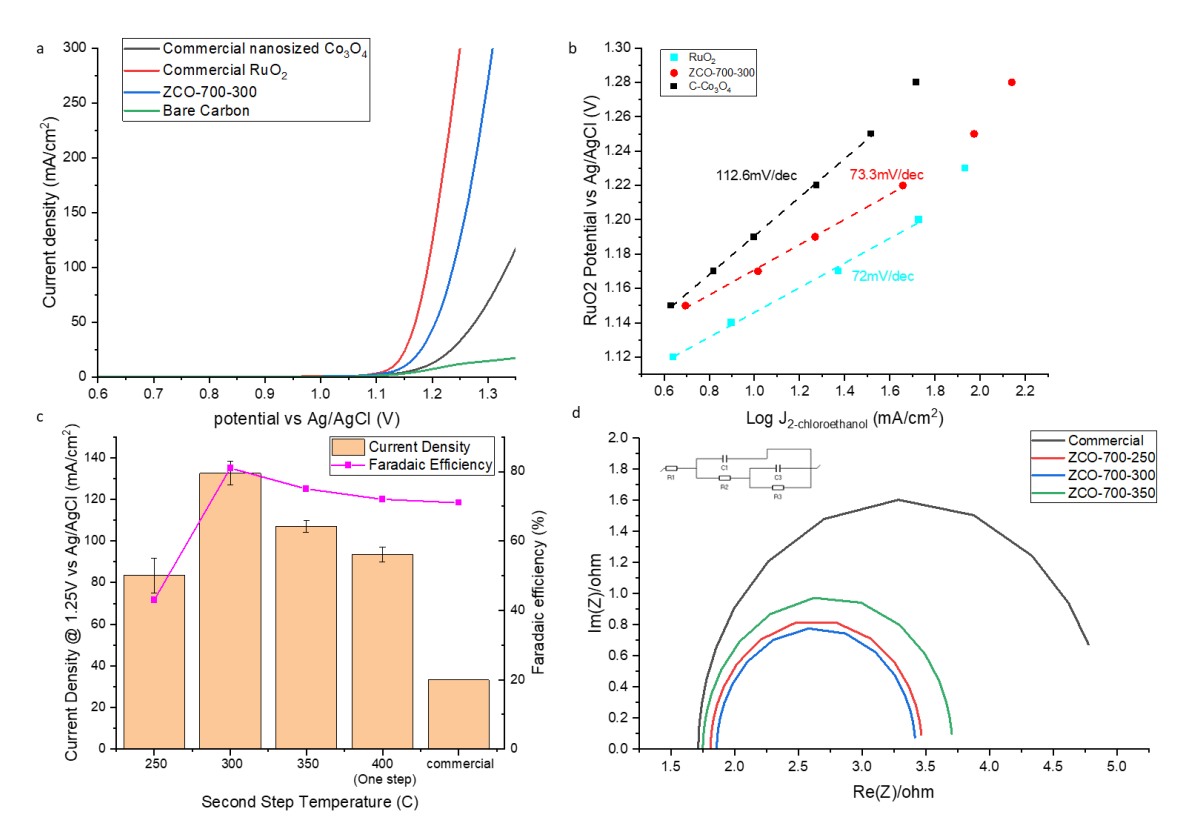


Figure 3. CIER performance of a) LSV test, b) Tafel slope, c) Current density and FE of samples prepared by different temperatures, d) EIS test (equivalent circuit inserted).

exhibited an outstanding performance for CIER, and careful control over the second step calcination temperature at 300 °C is critical for optimizing the CIER activity and selectivity. The performance for CIER reached lowest potential at 100 mA/cm² compared to other cobalt oxide catalyst and even comparable to some noble metal catalysts, as shown in **Table S2**.

The intrinsic activity was also examined by comparing their specific activity. However, it is challenging to quantify the Co₃O₄ surface area in ZCO-700-300. As we use either the nitrogen physisorption (i.e., BET) method or the double-layer capacitance method, we always obtain the total areas of both carbon and Co₃O₄. Instead, we used chemical surface area (CSA) to calculate the area-specific activity of CIER of our reported catalysts to compare their intrinsic activity. ZCO-700-300, C-Co₃O₄, and C-Co₃O₄ mixed with the same nitrogen doped carbon in ZCO-700-300 was examined (C-Co₃O₄-NC). As shown in Figure S9, C-Co₃O₄-NC showed similar performance compared to C-Co₃O₄. The specific activity of ZCO-700-300 is about 50% better than C-Co₃O₄ and C-Co₃O₄-NC. The possible reason could be attributed to 1) the heterojunction formed between carbon and Co₃O₄ during MOF calcination facilitated the electron transfer; 2) Co₃O₄ particles in ZCO-700-300 was separated by carbon, which increase the utilization of particle surface area.

Furthermore, the durability of $\text{Co}_3\text{O}_4/\text{NC}$ was evaluated at the constant current density of 100 mA/cm^2 for 10-hour electrolysis. The electrolyte was replaced by fresh electrolytes at each 2-hour interval to compensate for the consumption of reactant Cl⁻. The electrolysis was carried out in both 0.2 M phosphate-buffered electrolyte at pH

of 6 and unbuffered 2 M KCl electrolyte. Buffered solution pH was set to 6 because it is the highest pH in which HClO is the dominant species 23 . When the electrolyte pH is > 6, ClO $^{-}$ ion would be the dominant species that could not oxidize ethylene to ethylene chlorohydrin. Whether in the buffered or unbuffered system, ZCO-700-300 maintained a remarkably stable performance in terms of both low cell potential and high FE to EO (Fig. 4a). ICP-MS confirmed a very trace number of cobalt ions in the buffered analyte (equal to <0.002% of Co₃O₄ leaching). In the unbuffered system, although the anolyte pH continuously decreased and eventually formed a strong acid environment, we did not observe significant dissolution of Co₃O₄ after 10-hour electrolysis (3.6% Co₃O₄ leaching obtained from ICP-OES results). The slow cobalt dissolution rate may benefit from effective protection of Co₃O₄ by the carbon residual^{24, 25}. The slightly lower FE_{EO} in the buffered system may be attributed to the use of phosphate-buffered electrolyte, which can enhance the OER activity as phosphate has been reported to be able to facilitate the protoncoupled electron transfer process^{26, 27}. In addition, in terms of thermodynamic potential, the acidic environment in the unbuffered system increased OER equilibrium potential (e.g., 0.876 V at pH 6 and 1.171V at pH 1), while the CIER potential was unchanged (no proton participated, 1.36 V in all pH). Therefore, the standard reduction potential difference is reduced from 0.484 V to 0.136 V when the pH is changed from 6 to 1, this can also explain slightly higher FEEO in the unbuffered electrolyte. To confirm the OER is the dominating side reaction, online gas chromatography (GC) was utilized to identify gas product and NMR was employed to identify soluble by-products. No signal of other C₂H₄ partial products was observed (Figure S10, S11). XPS was conducted to study the durability of ZCO-700-300 after 10Journal Name ARTICLE

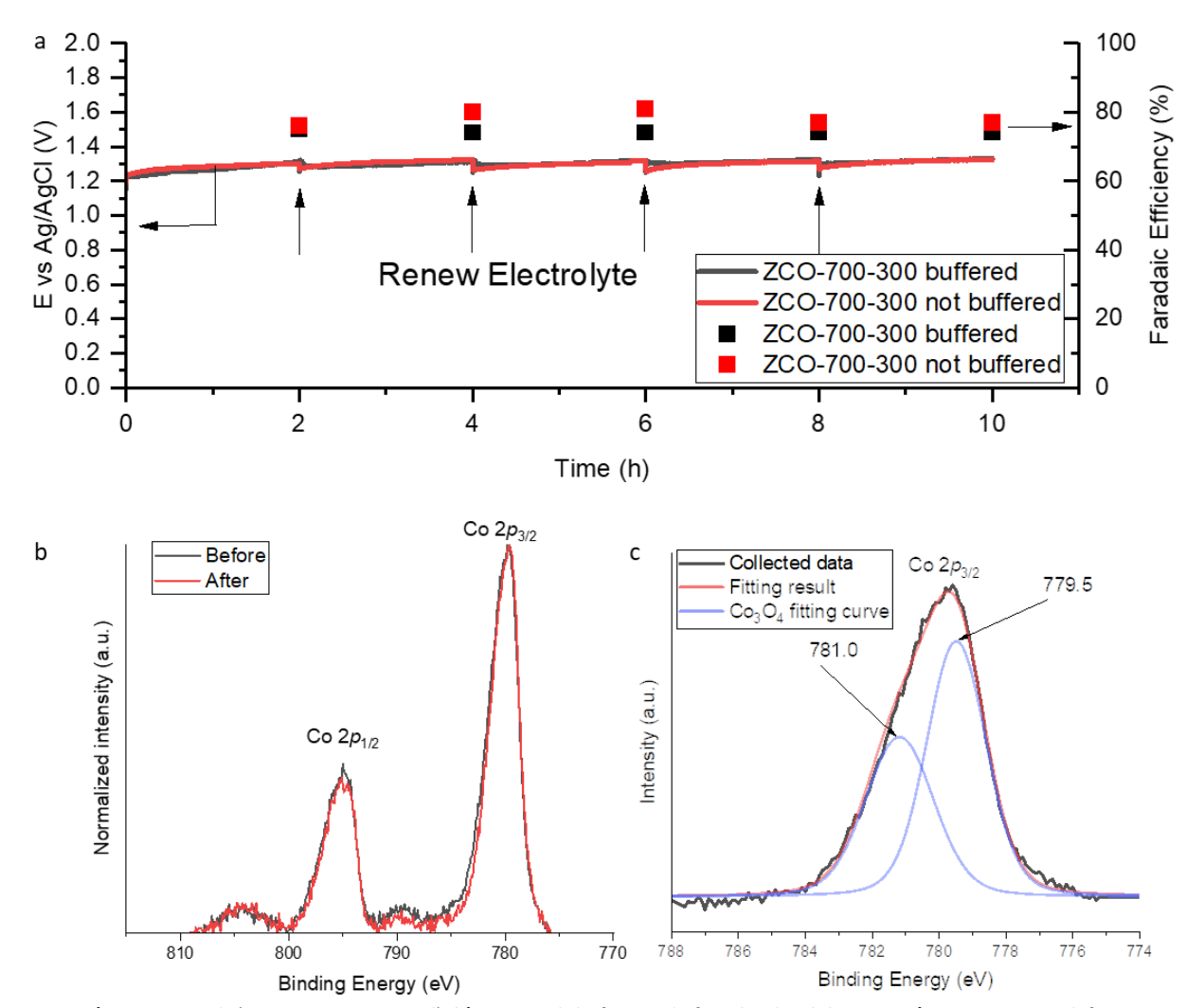


Figure 4. a) CP test result (90% IR compensated), b) XPS result before and after the durability test. c) Co₃O₄ 2p_{3/2} peak fitting curve,

hour electrolysis. Peaks at 779.5 and 781.0 eV in the XPS fitting curve can be assigned to Co^{3+} and Co^{2+} in Co_3O_4 , respectively. The overlapped XPS spectrum between the fresh catalyst (before the electrolysis) and spent catalyst (after 10-hour electrolysis) showed unchanged valence state of Co (Fig. 4b, 4c), which indicated the robust durability of $\text{Co}_3\text{O}_4/\text{NC}$ catalyst.

Conclusions

In summary, we have demonstrated MOF-derived $\text{Co}_3\text{O}_4/\text{NC}$ through our self-developed two-step calcination method can serve as a highly active catalyst for chlorine-assisted production of ethylene oxide. The effects of calcination method and temperature on the CIER activity and FE_{EO} on the ZCO samples were investigated and optimized. Benefitting from the porous structure with more exposed active sites and improved charge transfer, high CIER activity was obtained on $\text{Co}_3\text{O}_4/\text{NC}$ catalyst, which is comparable to a commercial RuO_2 catalyst. In the 10-hour chronoamperometry test, the optimized $\text{Co}_3\text{O}_4/\text{NC}$ catalyst exhibited remarkable stability in buffered electrolyte, in terms of CIER activity, FE_{EO} , and catalyst

phase stability. The strategy to synthesizing the MOF-derived Co3O4/NC materials could be used for the synthesis of efficient catalysts for other electrochemical reactions.

Experimental Methods

Materials and chemicals

All materials and chemicals were used as received without further purification. Platinum foil (25 x 25 x 0.025 mm, 99.99%) was purchased from Strem Chemicals Inc. Cobalt(II) nitrate hexahydrate (Co(NO3)2•6H2O, 98%), 2-Methyl Imidazole (2-MIM, 99%), ethylene oxide (EO, 50mg/mL in methanol), dimethylmalonic acid (DMMA, 99%) were purchased from Sigma-Aldrich. Potassium Chloride (KCI, 99%), ethylene glycol (EG) was purchased from Fisher Chemicals. Anion exchange membrane (AEM, Fumasep FAA-3-50) was purchased from Fuel Cell Store. Commercial Co₃O₄ was purchased from US Nano Research, Inc. Commercial RuO₂ was purchased from Premetek Co.

Preparation of precursor ZIF-67

The precursor ZIF-67 was synthesized by hydrothermal method²¹. Typically, 0.45g Co(NO₃)₂•6H₂O was dissolved into 3 mL of deionized (DI) water, and 5.5g of 2-methylimidazole (2-MIM) was dissolved into 20 mL of DI water separately. Then cobalt nitrate solution was added into 2-MIM solution slowly under stirring. The solution was kept stirring for 6 hours at room temperature. The purple precipitate was collected by centrifuging at 8000 rpm for 15 min and washed with water and methanol, respectively. The obtained precipitate was dried in a vacuum oven at 80 °C for 24 hours.

Preparation of ZCO samples

ZIF-derived cobalt oxide (ZCO) samples were prepared through a two-step calcination method (**Fig. 1b**). The first step calcination was conducted at 700 °C in a tube furnace under an argon atmosphere for 1 hour²⁸. The second step was performed in a muffle furnace under an air atmosphere for 1 hour at different temperatures of 250, 300, and 350 °C to study the temperature effect on samples' activity. To compare the effect of the calcination method, samples made by the one-step calcination method were also prepared at 350 and 400 °C under an air atmosphere.

Preparation of C-Co₃O₄-NC samples

ZIF-8 is a similar MOF as compared to ZIF-67, which replaces Co by Zn as the metal source. We chose ZIF-8 instead of ZIF-67 because Zn is easier to be removed, so we can obtain the nitrogen-doped carbon (without metal). ZIF-8 was then synthesized with the same molar ratio of metal ion to the organic linker as the ZIF-67 (reported in this work). The product was calcinated in Ar at 700 °C for 1 hour with a temperature ramp of 5 °C/min. The product after calcination is denoted as Zn/NC composite, which should be similar to ZCO-700-NA. Then Zn/NC was soaked in 0.5 M H₂SO₄ overnight to remove Zn²⁹. The remaining Zn is <1 wt%, as confirmed by EDS. We mixed the ZIF-8 derived carbon with a commercial Co₃O₄ (C-Co3O4) with a 14: 86 weight ratio, same as that for ZCO-700-300 according to the TGA results shown in Table S1. The mixture was grounded and dispersed in isopropanol alcohol and sprayed on 1 x 1 cm² carbon paper to reach the Co3O4 loading of 1 mg/cm². This sample was named as C-Co₃O₄-NC.

Preparation of electrodes

Commercial nanosized cobalt oxide (C-Co₃O₄), commercial ruthenium oxide (RuO₂), and various self-prepared samples were loaded on hydrophilic carbon paper by spray coating. The spray ink was made of active content and isopropanol (IPA) at 5 mg/mL concentration. The amounts of catalyst were normalized to 1 mg/cm² of Co₃O₄ or RuO₂ according to TGA results. Commercial samples were directly sprayed on carbon paper. Self-prepared samples were loaded by spray coating their precursor (ZIF-67 for one-step and ZCO-700-NA for two-step method) on carbon paper followed by calcination at designed temperatures. This loading method would enhance the contact with carbon paper and prevent physical peel-off.

Characterization of samples

Scanning electron microscopy (SEM) images and energy dispersive spectroscopy (EDS) spectra were obtained from FEI Quanta 250 FE-SEM. X-ray diffraction (XRD) data were collected from the Rigaku SmartLab diffractometer, with Cu K α radiation (λ = 0.15418 nm) working at 40 kV and 44 mA. Transmission electron microscopy (TEM)

images were captured using a JEOL 200kV JSM-2100 scanning transmission electron microscope with a Gatan OneView 4K camera. X-ray photoelectron spectroscopy (XPS) was performed with a Kratos Amicus/ESCA 3400 instrument. Nitrogen physisorption was carried out on Micromeritics ASAP 2020 Surface Area and Porosity Analyzer. It needed to be noted that BET measured both carbon and Co₃O₄ surface area while carbon was inert in CIER. Temperatureprogrammed oxidation was completed on the Micromeritics AutoChem II chemisorption Analyzer. Leached cobalt during durability test was determined by inductively coupled plasma-optical emission spectrometer (ICP-OES) on PerkinElmer Optima 8000 ICP-OES instrument and Agilent Technologies 7700 Inductively coupled plasma mass spectrometry (ICP-MS). Gas product was identified by gas chromatography (SRI instrument 8610C #3) equipped with HayeSep D and MolSieve 5Å columns. A thermal conductivity detector was used to quantify H2, and a flame ionization detector was employed to detect CO₂ and possible gaseous side products.

Electrochemical tests

Electrochemical tests were conducted on a BioLogic VSP-300 electrochemical workstation. Measurements were carried out in a typical H-type cell with an additional absorbing vessel (Fig. S12). Anode was prepared as described in section 2.4. The cathode was platinum foil. A saturated Ag/AgCl electrode was utilized as a reference electrode. The electrolyte was 2 M KCl solution at both the anode and cathode. An anion exchange membrane was used to separate the two compartments of this cell. Ethylene gas was purged into anolyte through a gas diffuser. An additional compartment was added to capture the chlorine gas generated on the anode.

Linear sweep voltammetry (LSV) was conducted to evaluate the activity performance of CIER. The scanning rate of LSV was 5 mV/s. A 90% IR compensation was used to eliminate the effect of solution resistance. Electrochemical impedance spectroscopy (EIS) was measured at 1.15 V vs. Ag/AgCl electrode to measure charge transfer resistance. Chronopotentiometry (CP) mode was utilized to test the durability of the catalyst at 100 mA/cm². The electrolyte was replaced with fresh electrolyte solution every 2 hours during the durability test to compensate for the consumption of chloride ions.

Product quantification.

The amount of product was measured by nuclear magnetic resonance (NMR) on Bruker NEO 400 instrument. An internal standard method was employed to quantify the product 17 . Typically, the solution was made of 200 μ L D $_2$ O, 100 μ L 15mM DMMA solution, and 400 μ L anolyte. Quantity was obtained by calculating the peak area ratio of the product to the internal standard and comparing it to the calibration curve. Peak area was obtained in MestReNova software with auto phase and baseline correction. A calibration curve made from the known product concentration in 2M KCl solution was used to quantify the product. An example of the NMR result and calibration curves for EG and EO were shown in supplementary information (Fig. S11). Faradic efficiency was calculated by:

$$FE = \frac{2 \times F \times n}{Q}$$

Where F is faraday constant, 96485.33 C/mol; 2 is the number of electrons transferred when one ethylene molecule is oxidized to ethylene chlorohydrin; n is the total amount of product measured by

Journal Name ARTICLE

NMR; Q is the total amount of electrons transferred in the circuit during the whole reaction.

Active chlorine was tested by WaterWorks free chlorine test strip. The lower detection limit is 25ppm, corresponding to 2 C charge. Typically, the experiment was carried out at 100 mA for 2h, which was 720 C total charge. If the color change of the strip was not observed, we assumed all active chlorine was consumed through reacting with ethylene.

Calculation of specific activity

It is challenging to quantify the specific area as mentioned above. Instead, chemical surface area (CSA) is a good alternative to calculate the area-specific activity of CIER of our reported catalysts to compare their intrinsic activity. By using Debye-Scherrer equation, the average particle size of the metal nanoparticles could be estimated from the diffraction peak of an isolated crystal plan in XRD patterns. The average size of the $\rm Co_3O_4$ nanoparticles obtained is 8 nm. The TEM image also shows that the $\rm Co_3O_4$ particle size ranges from 5 – 13 nm. The specific surface area of $\rm Co_3O_4$ thus can be calculated by the following equation.

$$CSA = \frac{S}{m} = \frac{S}{\rho * V} = \frac{4 * \pi * r^2}{\rho * \frac{4}{\rho} \pi * r^3} = \frac{3}{\rho * r}$$

Where S is surface area of a spheric Co particle; m is mass; p is density of cobalt oxide (6.11g/cm³); V is volume of the particle, and r is radius of the particle. The total specific surface area of Co_3O_4 in ZCO-700-300 would be 122.75 m²/g. Then the current density based on geometric electrode surface area could be converted to the current density based on the specific surface area. The specific activity of ZCO-700-300 was 0.108 mA/cm², which is 60% greater than the specific activity of commercial Co3O4 (0.067 mA/cm²). Although the surface area of the Co_3O_4 particles cannot be all available to the reaction, we actually can compare the intrinsic activity between our MOF-derived Co_3O_4 with commercial Co3O4 sample, if we assume they have same catalyst utilization (electrochemical active surface area / specific surface area).

Author Contributions

T. Li synthesized and characterized MOF-derived Co_3O_4 materials, and conducted most of electrochemical tests. H. Liu helped with setting up electrochemical cells for initial electrochemical tests and data analysis. J. Yu and W. Huang performed the ICP-MS tests and data collection and analysis. Y. Chen helped with GC tests. W. Li proposed and supervised the research. T. Li, H. Liu and W. Li wrote the manuscript, and all authors discussed results and edited the manuscript.

Conflicts of interest

There are no conflicts to declare.

Acknowledgements

This work was supported by the NSF grant (EFMA 2132200). W. Li is grateful to his Herbert L Stiles Faculty Fellowship. We acknowledge fruitful discussions with Prof. Jean-Philippe

Tessonnier, Dr. Shuang Gu, Dr. Jungkuk Lee, Basil Rawah, Xiaopeng Liu, and Mohammad Albloushi. T. Li appreciates Dr. Boote Brett, Dr. Cady Sarah, Dr. Warren Straszheim, Dr. Arkady Ellern for their valuable trainings on TGA, NMR, SEM and EDS, and XRD, respectively. We thank Dr. Patrick Johnston, Dr. Tracy Stewart and Dr. Dapeng Jing for their assistance with ICP, TEM, and XPS characterizations.

Notes and references

‡ Footnotes relating to the main text should appear here. These might include comments relevant not central to the matter under discussion, limited experimental and spectral data, and crystallographic data.

References

- 1. Smith, S. Global and China Ethylene Oxide (EO) Industry Report, 2017–2021. Global Reports,; 2017.
- 2. Rebsdat, S.; Mayer, D., Ethylene Glycol. In *Ullmann's Encyclopedia of Industrial Chemistry*, 2000.
- 3. Weaver, D. G.; Smart, J., Ethylene Oxide Derivatives. Glycols and Ethanolamines. *Industrial & Engineering Chemistry* **1959**, *51* (8), 894-900
- 4. Herzberger, J.; Niederer, K.; Pohlit, H.; Seiwert, J.; Worm, M.; Wurm, F. R.; Frey, H., Polymerization of Ethylene Oxide, Propylene Oxide, and Other Alkylene Oxides: Synthesis, Novel Polymer Architectures, and Bioconjugation. *Chemical Reviews* **2016**, *116* (4), 2170-2243.
- 5. Lefort, T. E. Process for the production of ethylene oxide.
- 6. Bukhtiyarov, V. I.; Nizovskii, A. I.; Bluhm, H.; Hävecker, M.; Kleimenov, E.; Knop-Gericke, A.; Schlögl, R., Combined in situ XPS and PTRMS study of ethylene epoxidation over silver. *Journal of Catalysis* **2006**, *238* (2), 260-269.
- 7. van Hoof, A. J. F.; Hermans, E. A. R.; van Bavel, A. P.; Friedrich, H.; Hensen, E. J. M., Structure Sensitivity of Silver-Catalyzed Ethylene Epoxidation. *ACS Catalysis* **2019**, *9* (11), 9829-9839.
- 8. van Hoof, A. J. F.; Filot, I. A. W.; Friedrich, H.; Hensen, E. J. M., Reversible Restructuring of Silver Particles during Ethylene Epoxidation. *ACS Catalysis* **2018**, *8* (12), 11794-11800.
- 9. Jones, T. E.; Wyrwich, R.; Böcklein, S.; Carbonio, E. A.; Greiner, M. T.; Klyushin, A. Y.; Moritz, W.; Locatelli, A.; Menteş, T. O.; Niño, M. A.; Knop-Gericke, A.; Schlögl, R.; Günther, S.; Wintterlin, J.; Piccinin, S., The Selective Species in Ethylene Epoxidation on Silver. *ACS Catalysis* **2018**, *8* (5), 3844-3852.
- 10. Platzer, N., Chemistry and Technology of Basic Organic and Petrochemical Synthesis. Volume 1 and Volume 2. N. N. Lebedev, MIR Publishers, Moscow, 1984,333 and 305 pp. *Journal of Polymer Science Part C: Polymer Letters* **1986**, *24* (6), 293-293.
- 11. Chen, G.; Li, X.; Feng, X., Upgrading Organic Compounds through the Coupling of Electrooxidation with Hydrogen Evolution. *Angewandte Chemie International Edition* **2022**, *61* (42), e202209014.

 12. Leow Wan, R.; Lum, Y.; Ozden, A.; Wang, Y.; Nam, D.-H.; Chen, B.; Wicks, J.; Zhuang, T.-T.; Li, F.; Sinton, D.; Sargent Edward, H., Chloride-mediated selective electrosynthesis of ethylene and propylene oxides at high current density. *Science* **2020**, *368* (6496), 1228-1233.
- 13. Li, Y.; Ozden, A.; Leow, W. R.; Ou, P.; Huang, J. E.; Wang, Y.; Bertens, K.; Xu, Y.; Liu, Y.; Roy, C.; Jiang, H.; Sinton, D.; Li, C.; Sargent, E. H., Redox-mediated electrosynthesis of ethylene oxide from CO2 and water. *Nature Catalysis* **2022**, *5* (3), 185-192.

- 14. Menzel, N.; Ortel, E.; Mette, K.; Kraehnert, R.; Strasser, P., Dimensionally Stable Ru/Ir/TiO2-Anodes with Tailored Mesoporosity for Efficient Electrochemical Chlorine Evolution. *ACS Catalysis* **2013**, *3* (6), 1324-1333.
- 15. Ha, H.; Jin, K.; Park, S.; Lee, K.-G.; Cho, K. H.; Seo, H.; Ahn, H.-Y.; Lee, Y. H.; Nam, K. T., Highly Selective Active Chlorine Generation Electrocatalyzed by Co3O4 Nanoparticles: Mechanistic Investigation through in Situ Electrokinetic and Spectroscopic Analyses. *The Journal of Physical Chemistry Letters* **2019**, *10* (6), 1226-1233.
- 16. Xiong, Q.; Zhang, X.; Cheng, Q.; Liu, G.; Xu, G.; Li, J.; Ye, X.; Gao, H., Highly selective electrocatalytic Cl– oxidation reaction by oxygen-modified cobalt nanoparticles immobilized carbon nanofibers for coupling with brine water remediation and H2 production. *Nano Research* **2020**, *14* (5), 1443-1449.
- 17. Chung, M.; Jin, K.; Zeng, J. S.; Manthiram, K., Mechanism of Chlorine-Mediated Electrochemical Ethylene Oxidation in Saline Water. *ACS Catalysis* **2020**, *10* (23), 14015-14023.
- 18. Li, J.; Chen, M.; Cullen, D. A.; Hwang, S.; Wang, M.; Li, B.; Liu, K.; Karakalos, S.; Lucero, M.; Zhang, H.; Lei, C.; Xu, H.; Sterbinsky, G. E.; Feng, Z.; Su, D.; More, K. L.; Wang, G.; Wang, Z.; Wu, G., Atomically dispersed manganese catalysts for oxygen reduction in proton-exchange membrane fuel cells. *Nature Catalysis* **2018**, *1* (12), 935-945.
- 19. Chen, L.; Ye, J.-W.; Wang, H.-P.; Pan, M.; Yin, S.-Y.; Wei, Z.-W.; Zhang, L.-Y.; Wu, K.; Fan, Y.-N.; Su, C.-Y., Ultrafast water sensing and thermal imaging by a metal-organic framework with switchable luminescence. *Nature Communications* **2017**, *8* (1), 15985.
- 20. Chong, L.; Wen, J.; Kubal, J.; Sen, F. G.; Zou, J.; Greeley, J.; Chan, M.; Barkholtz, H.; Ding, W.; Liu, D.-J., Ultralow-loading platinum-cobalt fuel cell catalysts derived from imidazolate frameworks. *Science* **2018**, *362* (6420), 1276-1281.
- 21. Qian, J.; Sun, F.; Qin, L., Hydrothermal synthesis of zeolitic imidazolate framework-67 (ZIF-67) nanocrystals. *Materials Letters* **2012**, *82*, 220-223.
- 22. Babar, P. T.; Lokhande, A. C.; Pawar, B. S.; Gang, M. G.; Jo, E.; Go, C.; Suryawanshi, M. P.; Pawar, S. M.; Kim, J. H., Electrocatalytic performance evaluation of cobalt hydroxide and cobalt oxide thin films for oxygen evolution reaction. *Applied Surface Science* **2018**, *427*. 253-259.
- 23. Ghernaout, D., Disinfection and DBPs Removal in Drinking Water Treatment: A Perspective for a Green Technology. *International Journal of ADVANCED AND APPLIED SCIENCES* **2018**, *5*, 108-117.
- 24. Senthil Raja, D.; Cheng, P.-Y.; Cheng, C.-C.; Chang, S.-Q.; Huang, C.-L.; Lu, S.-Y., In-situ grown metal-organic framework-derived carbon-coated Fe-doped cobalt oxide nanocomposite on fluorine-doped tin oxide glass for acidic oxygen evolution reaction. *Applied Catalysis B: Environmental* **2022**, *303*, 120899.
- 25. Singh, V.; Nagaiah, T. C., In situ incorporation of cobalt nanoclusters and nitrogen into the carbon matrix: a bifunctional catalyst for the oxygen depolarized cathode and chlorine evolution in HCl electrolysis. *Journal of Materials Chemistry A* **2019**, *7* (16), 10019-10029.
- 26. Jin, K.; Seo, H.; Hayashi, T.; Balamurugan, M.; Jeong, D.; Go, Y. K.; Hong, J. S.; Cho, K. H.; Kakizaki, H.; Bonnet-Mercier, N.; Kim, M. G.; Kim, S. H.; Nakamura, R.; Nam, K. T., Mechanistic Investigation of Water Oxidation Catalyzed by Uniform, Assembled MnO Nanoparticles. *Journal of the American Chemical Society* **2017**, *139* (6), 2277-2285.
- 27. Surendranath, Y.; Kanan, M. W.; Nocera, D. G., Mechanistic Studies of the Oxygen Evolution Reaction by a Cobalt-Phosphate Catalyst at Neutral pH. *Journal of the American Chemical Society* **2010**, *132* (46), 16501-16509.

- 28. Liu, M.; Zhang, M.; Zhang, P.; Xing, Z.; Jiang, B.; Yu, Y.; Cai, Z.; Li, J.; Zou, J., ZIF-67-Derived Dodecahedral Co@N-Doped Graphitized Carbon Protected by a Porous FeS2 Thin-Layer as an Efficient Catalyst to Promote the Oxygen Reduction Reaction. *ACS Sustainable Chemistry & Engineering* **2020**, *8* (10), 4194-4206.
- 29. Liang, P.; Wang, Q.; Kang, J.; Tian, W.; Sun, H.; Wang, S., Dualmetal zeolitic imidazolate frameworks and their derived nanoporous carbons for multiple environmental and electrochemical applications. *Chemical Engineering Journal* **2018**, *351*, 641-649.